Understanding Charge Transfer at PbS-Decorated Graphene Surfaces toward a Tunable Photosensor

Dayong Zhang, Lin Gan, Yang Cao, Qing Wang, Limin Qi, and Xuefeng Guo**

The phenomenon of charge transfer between active components and graphene has been extensively investigated in order to control the doping effects, improve the device performance, or develop new functional optoelectronic devices for potential applications in diverse areas ranging from energy conversion to catalysis and chemical/biological sensors.[1,2] A feature of particular interest is the inherent ultrasensitivity of graphene that arises from its active surface being exposed to the environment. Any small charge disturbances from the environment could cause drastic changes in its electrical properties. In conjunction with its high conductivity, high chemical stability, and ease of micro/nanofabrication, the inherent ultrasensitivity places graphene as a promising platform for creating new types of sensors and optoelectronic devices.[3–9] In this context, considerable interest has been very recently attracted to the incorporation of semiconductor quantum dots (QDs) (e.g. CdSe,[10,11] CdS,[12,13] Fe_3O_4,[14,15] CdTe,[16,17] TiO_2,[18,19] NiO,[20] Co_3O_4,[21] Mn_3O_4,[22] and so on) to form graphene-QD hybrid nanocomposites (Ref. 2 and references therein). This is because QDs show the size-dependent optical properties and unique compatibility to form heterostructures with solid conductors or semiconductors. The synergetic effects of excellent photoinduced charge separation abilities of QDs and remarkable electronic transport properties of graphene make these hybrid materials as potential candidates for developing high-performance next-generation optoelectronic devices. In most cases, however, graphene derivatives (GD), such as graphene oxide or reduced graphene oxide, were used because of their solution processibility. To date, very few studies have examined the intrinsic mechanisms of charge injection, regeneration, and recombination at pristine graphene-QD interfaces.[23–26] This might lead to ambiguous understanding of charge transfer mechanisms between these nanomaterials and graphenes, and incomplete use of intrinsic charge transport properties of pristine graphenes, such as ballistic ambipolar transport behaviors. In this study, we demonstrate a straightforward design of studying photoinduced charge transfer reactions from PbS QDs to graphene using high-quality CVD-grown single-layer graphenes (SLGs), thus leading to a reversible photoswitch with fine-tunability (**Figure 1**a). Remarkably, on the basis of deeper understanding of intrinsic hole transfer mechanism, the symmetric mirror-imaging photoswitching effects are rationally realized for the first time using a single pristine ambipolar SLG when the different gate fields are applied.

We chose PbS QDs as light absorbers because they display a superior quantum-confined bandgap that can be easily extended into the visible region or even the infrared for solar cells and photovoltaics.[27,28] The unique feature of these quantum dots we want to use is that light irradiation generates free electrons (e^-) and holes (h^+) as the active centers over the entire nanocrystals. By using graphenes as local probes, we intend to investigate intrinsic charge transfer at the graphene-PbS interface in combination with photoexcitation and the possibility of modulating the electrical properties of individual graphene sheets. To do this, high-quality CVD-grown SLG-based transistors were fabricated using a nondestructive method through a polymer-mediated transfer technique and selective oxygen plasma etching developed elsewhere (Figure 1a,b).[29] This method allows to mass-produce SLG transistor arrays with high yield. From the Raman spectrum of the CVD-grown graphene used (Figure 1c), a single symmetric 2D peak (~2680 cm^{-1}), a small G/2D ratio, and a negligible D peak were observed, which indicates that our graphene is a single layer with high quality.[30,31] After the initial electrical characterization, we deposited PbS thin films with different thicknesses (from 1 to 5 nm in 1-nm steps) on graphene surfaces by electron beam (e-beam) thermal evaporation.[32] High-resolution transmission electron microscopic (HRTEM) investigations reveal that PbS thin films consist of numerous PbS nanoparticles in the cubic polycrystalline form (Figure 1d), which is consistent with selected-area electron diffraction (SAED) experiments where clear rings corresponding to uniform cubic-shaped PbS nanocrystals were also observed (Figure 1e).[33,34] For a 2 nm-thick PbS thin film as a representative, the average diameter of PbS QDs is about 5 nm (Figure 1d and S1). This corresponds to an energy bandgap of ~ 0.90 eV calculated from the formula proposed by Moreels et al.[35]

$$E_g = 0.41 + (0.0252d^2 + 0.283d)^{-1}$$

where E_g is the bandgap in unit of eV. The formation of polycrystalline PbS QDs with the useful energy bandgap implies the interesting optoelectronic properties of graphene-PbS hybrid devices in the visible region described below.

We found that the electrical properties of graphenes after PbS QD decoration became very sensitive to light. To eliminate possible artifacts from gate hysteresis, all of the current-voltage

Dr. D. Zhang, L. Gan, Y. Cao, Q. Wang, Prof. L. Qi, Prof. X. Guo
Center for Nanochemistry
Beijing National Laboratory for Molecular Sciences (BNLMS)
State Key Laboratory for Structural Chemistry of Unstable and Stable Species
College of Chemistry and Molecular Engineering
Peking University
Beijing 100871, P. R. China
E-mail: liminqi@pku.edu.cn; guoxf@pku.edu.cn
Prof. X. Guo
Department of Advanced Materials and Nanotechnology
College of Engineering
Peking University
Beijing 100871, P. R. China

DOI: 10.1002/adma.201104597

ADVANCED MATERIALS
www.advmat.de

www.MaterialsViews.com

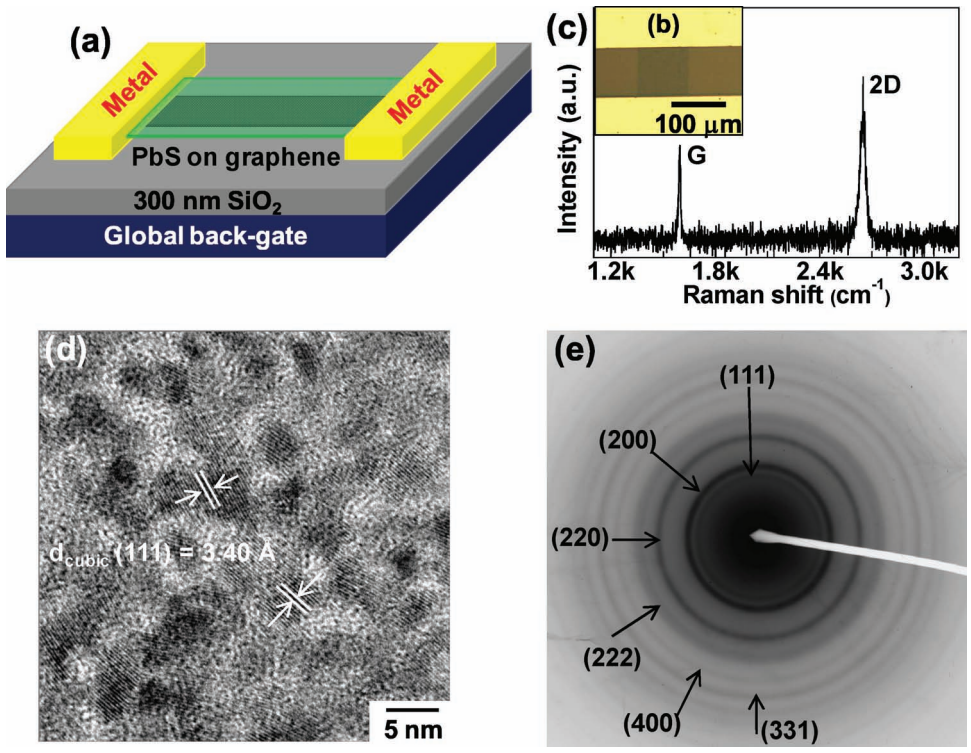

Figure 1. (a) Schematic representation of SLG transistors decorated by PbS thin films. (b) Optical image of a representative SLG device coated by a 2-nm PbS thin film. (c) Raman spectrum of high-quality CVD-grown graphenes. (d) HRTEM image of a 2-nm PbS membrane. (e) SAED pattern of the same PbS membrane.

curves (*I*–*V*) were acquired on the same measurement cycle while scanning from positive to negative bias. We observed very stable *I*–*V* curves for these devices in fixed experimental conditions, thus they can be used to detect the photoresponsive properties. We note that, due to chemical doping and charge transfer induced by etching agents and polymer resists (iron nitrate and polymethyl methracrylate),[29] the resulting graphenes only behave as p-type semiconductors (black curve in **Figure 2**a). To preclude the possibility of intrinsic photoresponses of graphenes, which could be measured by using high-intensity laser light for building ultrafast photodetectors,[36] we first detected the electrical properties of graphenes before PbS thin film deposition when visible light (150W halogen lamp) was switched on and off. We did not observe the obvious current changes under light irradiation (red curve in Figure 2a), even in the real-time measurements (black curve in Figure 2b). This sets the foundation for the following studies of charge transfer at the graphene-PbS interfaces. After PbS thin film deposition, the devices showed obvious conductance decrease (green curve in Figure 2a), most likely due to the scattering effect for carriers created by PbS thin films that are intimately covered on graphene surfaces, rather than the physical damages by the deposition process (Figure S2). We found that the photoresponsive behaviors of these graphene-PbS hybrid devices were thickness-dependent. With the increasing thickness of PbS thin films, the photocurrents varied when the devices were exposed to light in the same condition and showed the highest at the thickness of 2 nm (Figure S3). This is because charge transfer occurs at most at the surfaces of the active PbS QDs that are in close vicinity to graphene-PbS interfaces. It has been shown that photoinduced interfacial charge density, which is dependent on the quantity of photons absorbed in the active layer, does not smoothly increase as a function of active layer thickness, but is oscillatory because of the interference between forward and reflected radiation.[37,38] On the basis of this finding, to maximize photoinduced charge transfer at the interface, we determined to use graphene-PbS hybrid devices with the film thickness of 2 nm as a representative for the following investigations. Note that we failed to observe the obvious photoresponsive behaviors of graphene devices that were coated by oleylamine-encapsulated monodisperse colloidal PbS nanocrystals of different sizes synthesized from solution. This might be ascribed to the presence of oleylamine that blocks the pathway of sensitive charge transfer between PbS nanoparticles and graphene under light irradiation.

Figure 2a,b show the changes in the electrical characteristics for such a device under visible light irradiation and in the dark. Noticeably, upon light irradiation, obvious increase in source-drain current (I_D) occurred regardless of the gate bias (blue curve in Figure 2a). Previous studies demonstrated that the incident visible light generated delocalized electron–hole pairs over the entire PbS QDs.[27,28] As hypothesized by Dittrich et al.,[39] the photogenerated electrons in general have the large mobility and could behave as a Coulomb trap. For hole transport semiconductors, these active electrons can quench the p-type carriers and lead to the decrease of the device conductance.[40–42] However, the observation in the current case is completely opposite. Therefore, it is reasonable to deduce that, in

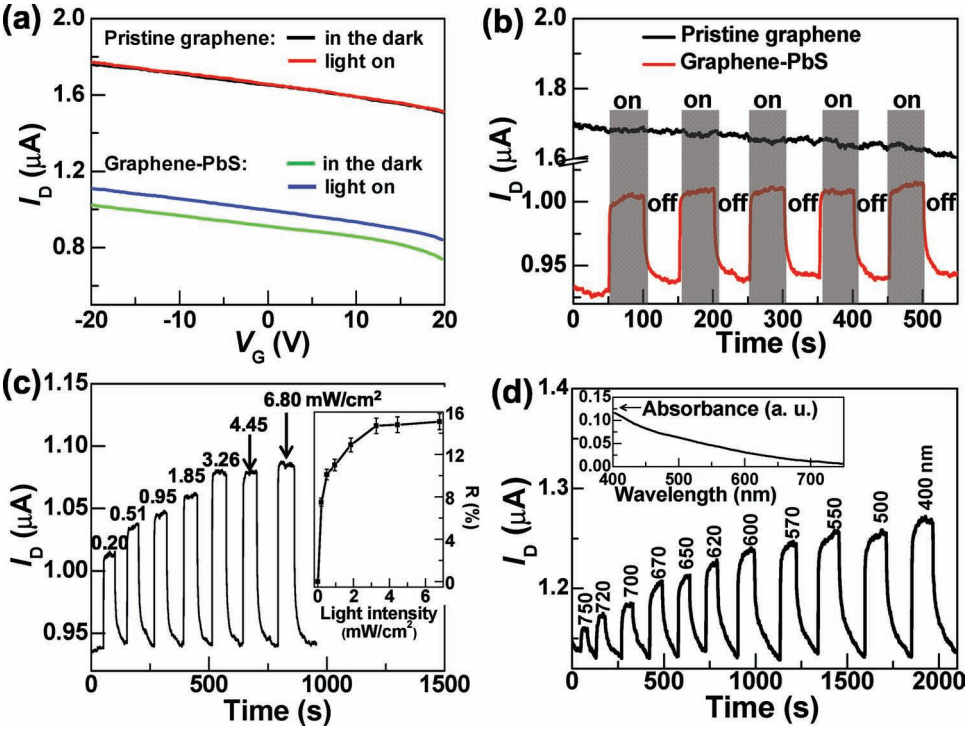

Figure 2. (a) Device characteristics of a representative device in each step of sequential operations. Black: pristine graphene in the dark; red: pristine graphene under light irradiation; green: PbS-decorated graphene in the dark; blue: PbS-decorated graphene under light irradiation. $V_D = 1$ mV. (b) The time trace of I_D for a PbS-decorated SLG while visible light was toggled on and off. $V_D = 1$ mV. $V_G = 0$ V. (c) I_D for the same device as lights of different power were switched on and off. Inset shows the power dependence of the changes in I_D. $V_D = 1$ mV. $V_G = 0$ V. (d) I_D for another device as lights of different wavelength were switched on and off. $V_D = 1$ mV. $V_G = 0$ V. Inset shows the UV-visible absorption spectrum of a 2-nm thick PbS thin film on quartz substrate.

contrast to previous hypothesis, the photogenerated holes could penetrate through the PbS-graphene interface to the conductive channel and thereby result in the p-type carrier mobility increase in these graphene-PbS hybrid devices (and the corresponding conductance enhancement) (**Figure 3**a). It should be mentioned that the fact we found here is different from similar observations reported in earlier work where electron transfer dominated the photocurrent of devices formed from QD-GD composites because quantum dots are the components contributing to the conductance.[10,11,17,18,20] Note that, control experiments demonstrated that only 2 nm-thick PbS thin films are insulating due to the uncontinuity. Remarkably, when kept in the dark after visible light irradiation, its drain current of the same device was essentially restored to its initial value. We found that the back-and-forth photoswitching effect is quite fast in time. The red curve in Figure 2b shows five representative switching cycles of the same device when visible light was switched on and off. The drain current sharply increased to the saturation within ~1 s of exposure when PbS thin films reached the maximum of photogenerated charge separation. On the contrary, after the high-conductance state was established and the device was kept in the dark, the device presented a fast current relaxation, completing the decrease after ~10 s. This can be explained by the fast charge recombination on the surface of PbS thin films by holes that originate from the conductive channel where the p-type transistors have a very high density of holes. To rule out potential artifacts from Schottky barrier modification, we performed control experiments using graphene devices with narrowed PbS thin films that were disconnected with metal electrodes as demonstrated in Figure S4. We did observe the similar photoswitching effect. In combination with two aforementioned control experiments (using pure graphenes and pure PbS thin films), these results consistently prove that that the photoactivity of PbS QDs immobilized on the surface of graphenes is responsible for the changes in device characteristics as discussed above, rather than a local change at the metal–graphene junctions and subsequent Schottky barrier height modulation. These photoswitching phenomena are quite reproducible as the yield of working devices is very high (at least 45 working devices out of 48 original PbS-decorated graphene devices).

Figure 2c shows the power dependence of the photocurrent of the same device used in Figure 2a. With the increase of light power, the drain current (I_D) of the device gradually saturates, indicating that the photoinduced carrier separation has reached its maximum. To further understand the important role of PbS QDs in device photoconductivity, we carried out wavelength-dependent measurements. Figure 2d shows the current data of another similar device as a function of light wavelength at fixed S/D (V_D) and gate (V_G) biases. Interestingly, we found that the changes in I_D showed the gradual increase with the decrease of light wavelength, consistent with the UV/vis absorption spectrum of 2-nm thick PbS films deposited by thermal evaporation on quartz substrates. These results clearly demonstrated the fact that PbS QDs decorated on graphene surfaces do play

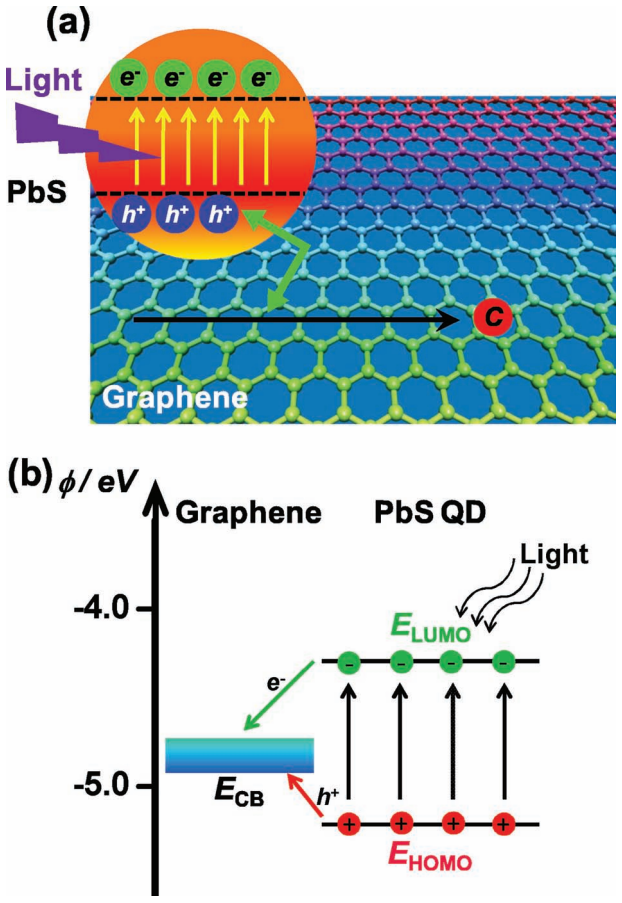

Figure 3. (a) Mechanistic illustration of the hybrid devices when exposed to light. (b) Schematic representation of energy levels for graphene and PbS DQs used. Red and green arrows represent desired and undesired charge transport processes, respectively.

the key role in device photocurrent. Furthermore, varying light power and wavelengths results in the gradual enhancement of the photocurrents, forming the basis for new types of optoelectronic devices and sensors with the fine-tunability. By using the conventional model for the responsivity (R_{ill}) calculation [$R_{ill} = I_{ph}/(I_{ill}LW) = (|I_l - I_{dark}|)/(I_{ill}LW)$], where I_{ph} is the photocurrent, I_l the drain current under illumination, I_{dark} the drain current in the dark, I_{ill} the light power intensity, L the channel length of the device, and W the channel width of the device, the calculated value at the wavelength of 400 nm is ~8.4 A W^{-1}, which is comparable to conventional photodetectors (typically < 10 A W^{-1}), while the device was held at V_G = 0 V and V_D = 1 mV (I_{ill} = 175 μW cm^{-2}, W = 100 μm and L = 100 μm). There are two possible synergistic mechanisms for photoconductivity in the graphene-PbS hybrid devices: the photoinduced carrier separation of PbS nanoparticles and the carrier injection from PbS nanoparticles to graphene. Under light illumination, the photogenerated holes are created over the entire nanocrystals because the optical energy ($h\nu$) is larger than the energy band (E_g) of PbS nanoparticles and collected at the graphene-PbS interfaces.[27,28] The second mechanism simultaneously operative for the photoconductive gain is the efficient injection of these photogenerated holes from PbS nanoparticles to graphene through the graphene-PbS interfaces.[2–4] Together these two effects cause an increase in channel carrier concentration that contributes to the photocurrents under a S/D bias (V_D). On the basis of the equation used for calculating the current per unit width ($K = I_D/W = \mu_g Q_n V_D/L$),[43] where μ_g is the effective mobility for carriers in graphene and Q_n the magnitude of the areal charge density of graphene, we can deduce that the photocurrent (I_{ph}) is determined by $I_{ph} = \mu_g \Delta Q_n V_D W/L$, considering that μ_g itself remains constant before and after light illumination in the current case. This implies that I_{ph} is proportional to μ_g under the same illumination condition and at the fixed bias voltages. Therefore, in conjunction with both aforementioned mechanisms, the fact that CVD-grown graphenes show the high mobility ($\mu_g \geq 1000$ cm^2 V^{-1} s^{-1})[29,44] produces the high photoresponsivity of the devices.

To further understand the intrinsic unusual hole transfer mechanism, we show the key interfacial charge transfer processes occurring at graphene-PbS interfaces in Figure 3b. The lowest unoccupied molecular orbital (LUMO) energy of PbS QDs can be estimated using the following zeroth-order approximation of the effective-mass model:[45]

$$E_{LUMO} = E_{CB}(\text{bulk}) + (E_g(\text{QD}) - E_g(\text{bulk}))[m_h/(m_h + m_e)]$$

where E_{CB}(bulk) is the bulk conduction band energy (versus vacuum), E_g(QD) and E_g(bulk) are the PbS QD and bulk bandgaps, and m_h and m_e are the effective hole and electron masses in the bulk semiconductor. Using the values E_{CB}(bulk), E_g(bulk), m_h, and m_e in PbS according to the literature,[46,47] we calculated a LUMO energy of ca. –4.30 eV (relative to vacuum) for PbS QDs with the average diameter of 5 nm, and a highest occupied molecular orbital (HOMO) level of ca. –5.20 eV, slightly lower than those obtained experimentally.[48] We suggest that the photoexcitation of PbS QDs activates PbS ground-state electrons into the excited states and then form electron–hole pairs at their surface. Because the work function of graphene is 4.7–4.9 eV,[49,50] which is closer to the valence band of PbS QDs, the photogenerated holes can be efficiently injected to the conductance band of graphenes, thus leading to an increase of the hole carrier density (and the corresponding conductance) in a p-type semiconductor. On the contrary, the photgenerated electrons are trapped on the surface of PbS nanoparticles. As electrons and holes have a similar effective mass in PbS, changes in confinement energy upon changing QD size should be evenly apportioned in shifting the HOMO and LUMO energies, which we believe is a promising strategy to optimize the hole injection efficiency.

On the basis of the deep understanding of the intrinsic charge transfer mechanism, it can be further inferred that we should observe both a hole current increase and electron-current decrease in the same device when an ambipolar material is used. To prove this prediction, we decided to use pristine ambipolar SLGs formed with a peeling-off technique,[50] which show both electron and hole transport properties. By following the same sequential steps, we recorded the device characteristics of the ambipolar devices as represented in **Figure 4**a. A set of *I–V* curves are shown in Figure 4b, indicating the obvious positive shift of the Dirac point due to photoinduced p-type doping. Figure 4c shows the time traces of I_D when the same device was held at different gate bias voltages. Similarly, a significant hole current increase was observed under visible light

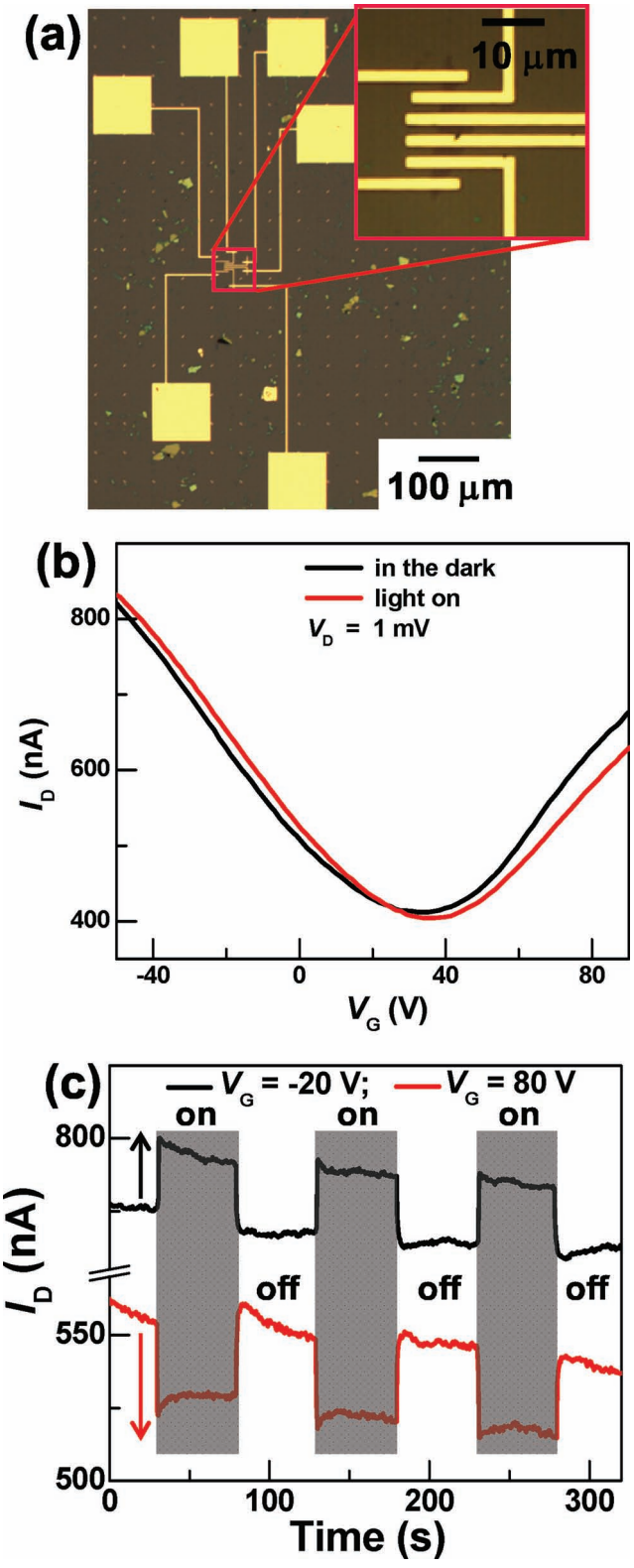

Figure 4. (a) Optical images of a representative device with 2-nm PbS thin films using pristine graphenes formed by a peeling-off technique. (b) Device characteristics of a representative device with 2-nm PbS thin films using pristine graphenes formed by a peeling-off technique under light irradiation and in the dark. V_D = 1 mV. (c) Time traces of I_D when the device was held at different gate bias voltages. V_D = 1 mV.

irradiation when V_G was held at –20 V, and the photoswitching process was reversible when light was switched on and off. Remarkably, when V_G was applied at 80 V, we observed, as expected, a fast reversible current decrease in the same device in the same irradiation condition. These results are reasonable because photoinduced free holes of PbS QDs can increase the hole current in the p-type materials and have an opposing function as the Coulomb traps to scatter the electron carriers in the n-type semiconductors. In the control experiments, we did not observe obvious changes in drain current no matter what kind of the gate bias (either negative or positive) was applied (Figure S5). It is worthwhile to emphasize that rational control of the photoactivity of PbS realizes symmetric, opposing photoswitching effects, which are effectively mirror images, using the same pristine graphene sheet. Noticeably, we found that the calculated device responsivities (R_{ill}) are quite high, ~2.8×10^3 A W^{-1} at the negative gate bias and ~1.7×10^3 A W^{-1} at the positive gate bias (I_{ill} = ~200 μW cm^{-2}, W = ~3 μm and L = ~3 μm at V_D = 1 mV), respectively.

In summary, this study details a direct design to understand intrinsic charge transfer mechanisms at the graphene-QD interface using pristine SLGs as local probes in combination with photoexcitation. Interestingly, we found an unusual phenomenon of photoinduced hole transfer reactions from PbS to graphene. The photoinduced free holes of PbS QDs can be injected efficiently into the conductive channel, thus increasing the hole carrier density in the p-type materials and, on the contrary, functioning as Coulomb traps to scatter the electron carriers in n-type semiconductors. It is remarkable that rational utilization of this finding not only leads to a reversible photosensor with fine-tunability and high responsivity, but also realizes mirror-image photoswitching effects in a single graphene device. We believe that these results provide a deeper understanding of interfacial phenomena and offer new attractive insights for building future ultrasensitive devices for applications such as light detection, sensing, imaging, optical communication, and memory storage.

Supporting Information

Supporting Information is available from the Wiley Online Library or from the author.

Acknowledgements

We acknowledge primary financial support from MOST (2009CB623703 and 2012CB921404), NSFC (20833001, 50873004, 51121091, 2112016, and 21073005), and FANEDD (2007B21).

Received: December 1, 2012
Revised: February 22, 2012
Published online: April 16, 2012

[1] W. R. Yang, K. R. Ratinac, S. P. Ringer, P. Thordarson, J. J. Gooding, F. Braet, *Angew. Chem. Int. Ed.* **2010**, *49*, 2114.
[2] X. Huang, X. Qi, F. Boey, H. Zhang, *Chem. Soc. Rev.* **2012**, (DOI: 10.1039/c1cs15078b, "41, 666").
[3] A. K. Geim, K. S. Novoselov, *Nat. Mater.* **2007**, *6*, 183.

[4] A. K. Geim, *Science* **2009**, *324*, 1530.
[5] C. N. R. Rao, A. K. Sood, K. S. Subrahmanyam, A. Govindaraj, *Angew. Chem. Int. Ed.* **2009**, *48*, 7752.
[6] F. Schwierz, *Nat. Nanotechnol.* **2010**, *5*, 487.
[7] K. P. Loh, Q. L. Bao, P. K. Ang, J. X. Yang, *J. Mater. Chem.* **2010**, *20*, 2277.
[8] D. Wei, Y. Liu, *Adv. Mater.* **2010**, *22*, 3225.
[9] Y. Cao, M. L. Steigerwald, C. Nuckolls, X. Guo, *Adv. Mater.* **2010**, *22*, 20.
[10] X. Geng, L. Niu, Z. Xing, R. Song, G. Liu, M. Sun, G. Cheng, H. Zhong, Z. Liu, Z. Zhang, L. Sun, H. Xu, L. Lu, L. Liu, *Adv. Mater.* **2010**, *22*, 638.
[11] Y. Lin, K. Zhang, W. Chen, Y. Liu, Z. Geng, J. Zeng, N. Pan, L. Yan, X. Wang, J. G. Hou, *ACS Nano* **2010**, *4*, 3033.
[12] A. Cao, Z. Liu, S. Chu, M. Wu, Z. Ye, Z. Cai, Y. Chang, S. Wang, Q. Gong, Y. Liu, *Adv. Mater.* **2010**, *22*, 103.
[13] H. Chang, X. Lv, H. Zhang, J. Li, *Electrochem. Commun.* **2010**, *12*, 483.
[14] X. Yang, X. Zhang, Y. Ma, Y. Huang, Y. Wang, Y. Chen, *J. Mater. Chem.* **2009**, *19*, 2710.
[15] Y. Zhan, X. Yang, F. Meng, J. Wei, R. Zhao, X. Liu, *J. Colloid Interface Sci.* **2011**, *363*, 98.
[16] J. Chu, X. Li, P. Xu, *J. Mater. Chem.* **2011**, *21*, 11283.
[17] Z. Lu, C. X. Guo, H. B. Yang, Y. Qiao, J. Guo, C. M. Li, *J. Colloid Interface Sci.* **2011**, *353*, 588.
[18] K. K. Manga, S. Wang, M. Jaiswal, Q. Bao, K. P. Loh, *Adv. Mater.* **2010**, *22*, 5265.
[19] G. Williams, B. Seger, P. V. Kamat, *ACS Nano* **2008**, *2*, 1487.
[20] H. Yang, G. H. Guai, C. Guo, Q. Song, S. P. Jiang, Y. Wang, W. Zhang, C. M. Li, *J. Phys. Chem. C* **2011**, *115*, 12209.
[21] Y. Y. Liang, Y. G. Li, H. L. Wang, J. G. Zhou, J. Wang, T. Regier, H. J. Dai, *Nat. Mater.* **2011**, *10*, 780.
[22] H. L. Wang, L. F. Cui, Y. A. Yang, H. S. Casalongue, J. T. Robinson, Y. Y. Liang, Y. Cui, H. J. Dai, *J. Am. Chem. Soc.* **2010**, *132*, 13978.
[23] Y.-T. Kim, J. H. Han, B. H. Hong, Y.-U. Kwon, *Adv. Mater.* **2010**, *22*, 515.
[24] Q. Wang, X. Guo, L. Cai, Y. Cao, L. Gan, S. Liu, Z. Wang, H. Zhang, L. Li, *Chem. Sci.* **2011**, *2*, 1860.
[25] H. Zhou, C. Qiu, Z. Liu, H. Yang, L. Hu, J. Liu, H. Yang, C. Gu, L. Sun, *J. Am. Chem. Soc.* **2010**, *132*, 944.
[26] J. Y. Son, Y.-H. Shin, H. Kim, H. M. Jang, *ACS Nano* **2010**, *4*, 2655.
[27] F. W. Wise, *Acc. Chem. Res.* **2000**, *33*, 773.
[28] E. H. Sargent, *Nat. Photonics* **2009**, *3*, 325.
[29] L. Gan, S. Liu, D. N. Li, H. Gu, Y. Cao, Q. Shen, Z. X. Wang, Q. Wang, X. F. Guo, *Acta Phys.Chim. Sin.* **2010**, *26*, 1151.
[30] M. S. Dresselhaus, A. Jorio, M. Hofmann, G. Dresselhaus, R. Saito, *Nano Lett.* **2010**, *10*, 751.
[31] M. A. P. L. M. Malard, G. Dresselhaus, M. S. Dresselhaus, *Phys. Rep.* **2009**, *473*, 51.
[32] S. Kumar, T. P. Sharma, M. Zulfequar, M. Husain, *Phys. B Condens. Matter* **2003**, *325*, 8.
[33] A. Mondal, N. Mukherjee, *Mater. Lett.* **2006**, *60*, 2672.
[34] E. C. Hao, B. Yang, S. Yu, M. Y. Gao, J. C. Shen, *Chem. Mater.* **1997**, *9*, 1598.
[35] I. Moreels, K. Lambert, D. Smeets, D. De Muynck, T. Nollet, J. C. Martins, F. Vanhaecke, A. Vantomme, C. Delerue, G. Allan, Z. Hens, *ACS Nano* **2009**, *3*, 3023.
[36] F. N. Xia, T. Mueller, Y. M. Lin, A. Valdes-Garcia, P. Avouris, *Nat. Nanotechnol.* **2009**, *4*, 839.
[37] L. A. A. Pettersson, L. S. Roman, O. Inganas, *J. Appl. Phys.* **1999**, *86*, 487.
[38] A. J. Moule, K. Meerholz, *Appl. Phys. B: Lasers Opt.* **2008**, *92*, 209.
[39] T. Dittrich, V. Duzhko, F. Koch, V. Kytin, J. Rappich, *Phys. Rev. B* **2002**, *65*, 155319.
[40] M. F. Calhoun, C. Hsieh, V. Podzorov, *Phys. Rev. Lett.* **2007**, *98*, 096402.
[41] S. Liu, J. M. Li, Q. Shen, Y. Cao, X. F. Guo, G. M. Zhang, C. Q. Teng, J. Zhang, Z. F. Liu, M. L. Steigerwald, D. S. Xu, C. Nuckolls, *Angew. Chem. Int. Ed.* **2009**, *48*, 4759.
[42] Q. Shen, Y. Cao, S. Liu, L. Gan, J. Li, Z. Wang, J. Hui, X. Guo, D. Xu, Z. Liu, *J. Phys. Chem. Lett.* **2010**, *1*, 1269.
[43] R. R. Troutman, A. Kotwal, *IEEE Trans. Electron Devices* **1989**, *36*, 2915.
[44] X. S. Li, W. W. Cai, J. H. An, S. Kim, J. Nah, D. X. Yang, R. Piner, A. Velamakanni, I. Jung, E. Tutuc, S. K. Banerjee, L. Colombo, R. S. Ruoff, *Science* **2009**, *324*, 1312.
[45] J. Jasieniak, J. Pacifico, R. Signorini, A. Chiasera, M. Ferrari, A. Martucci, P. Mulvaney, *Adv. Funct. Mater.* **2007**, *17*, 1654.
[46] S. Baskoutas, A. F. Terzis, *Mater. Sci. Eng., B* **2008**, *147*, 280.
[47] S. A. McDonald, G. Konstantatos, S. G. Zhang, P. W. Cyr, E. J. D. Klem, L. Levina, E. H. Sargent, *Nat. Mater.* **2005**, *4*, 138.
[48] B.-R. Hyun, Y.-W. Zhong, A. C. Bartnik, L. Sun, H. D. Abruna, F. W. Wise, J. D. Goodreau, J. R. Matthews, T. M. Leslie, N. F. Borrelli, *ACS Nano* **2008**, *2*, 2206.
[49] S. P. Pang, H. N. Tsao, X. L. Feng, K. Mullen, *Adv. Mater.* **2009**, *21*, 3488.
[50] Y. Cao, Z. Wei, S. Liu, L. Gan, X. Guo, W. Xu, M. L. Steigerwald, Z. Liu, D. Zhu, *Angew. Chem. Int. Ed.* **2010**, *49*, 6319.